International Journal on Recent and Innovation Trends in Computing and Communication
ISSN: 2321-8169 Volume: 11 Issue: 9
Article Received: 25 July 2023 Revised: 12 September 2023 Accepted: 30 September 2023

Implementation of Passivity-based Control of Four-Leg Inverter for Transformerless Three-Phase Solar Photovoltaic Systems

N. Uday Kumar[#1], M. Chakravarthy[*2], B. Mangu[#3]

[#1]Department of Electrical and Electronics Engineering, Vasavi College of Engineering, Hyderabad, Telangana

[*2]Professor, Department of Electrical and Electronics Engineering, Vasavi College of Engineering, Hyderabad, Telangana

[#3]Professor, Department of Electrical Engineering, Osmania University, Hyderabad, Telangana

e-mail: [#1]uday@staff.vce.ac.in, [*2]muktevchakri@staff.vce.ac.in, [#3]bmanguou@gmail.com

Abstract— This study explores the application of a passivity-based control technique (PBC) with an artificial neuro-fuzzy inference system (ANFIS) in a grid-connected Solar Photovoltaic (SPV) generating system for estimating reference grid currents. To optimise the tracking of the maximum power point (MPPT) between the solar photovoltaic (SPV) system and the DC bus, a DC – DC boost converter (BC) is utilised. This converter is connected to a four-leg, three-level neutral-point-clamped converter (4-leg 3L-NPC), interfaced with a three-phase, four-wire distribution system. The four-leg 4-leg 3L-NPC of the SPV generating system with Space vector pulse width modulation technique (SVPWM) is utilised for reducing common-mode voltage (CMV), leakage current (LC), reactive power for zero voltage regulation, power factor correction, load balancing, and the elimination of load harmonic currents in the proposed distribution system. The performance analysis of the proposed system is conducted on the Matlab/Simulink platform. Additionally, a comparative analysis is presented, contrasting the proposed system with a 3-phase 4-leg T-type neutral-point-clamped converter (TNPC) employing the PBC technique followed by ANFIS.

Keywords- Passivity-based Control(PBC), four-leg three-level converter, T-type neutral point clamped converter.

I. INTRODUCTION

In addressing the worldwide energy crisis, there has been notable interest in solar photovoltaic (SPV) systems in recent years [1, 2]. However, within urban settings, rooftop-mounted and building-integrated SPVs have moderate power capacities. To optimise the usage of power converters throughout the day, they can serve as active shunt compensators. Additionally, various types of loads, including fluorescent lamps, LED and CFL lighting, TVs, computers and other modern electrical devices, are commonly present in three-phase four-wire distribution systems in residential and office buildings at the PCC. The functioning of these elements can lead to suboptimal Power Quality, marked by issues such as inadequate power factor, imbalance, harmonics, and excessive neutral current in the AC mains. Optimise these Power Quality challenges arising from non-linear loads connected at the Point of Common Coupling (PCC), the power converters within SPV generating systems can undertake supplementary roles like reactive power compensation, load balancing, harmonics elimination, and mitigation of neutral current to address Power Factor Correction at the AC mains. This, in turn, leads to reduced losses and enhanced utilisation of distribution systems [3].

Traditional grid-connected SPV systems face challenges, including elevated installation expenses, reduced efficiency, and fluctuations in SPV output power due to changing solar irradiation. Furthermore, challenges pertaining to power quality, including power factor correction and compensation of neutral current, pose additional hurdles in grid-connected SPV networks [4–6]. Various MPPT techniques to improve the SPV system performance were extensively discussed in the literature [7–9].

Sophisticated control algorithms are essential for grid-interfaced SPV generating systems to incorporate functionalities including compensating for reactive power, balancing loads, eliminating harmonics, and mitigating neutral currents [10-11]. Different algorithms were addressed to govern active shunt compensators, encompassing theories like instantaneous reactive power theory, power balance theory, SRF theory, P-Q theory, 'Icosϕ,' and others [12-13].

An improved droop control method was developed with the goal of enhancing power-sharing and ensuring the stability of terminal voltages and system frequency for distributed generators (DGs) under both balanced and unbalanced loads [14]. The three-dimensional coordinate configuration was proposed, and it is responsible for powering stand-alone asymmetric loads, intending to preserve the equilibrium of the output capacitor voltages and achieve a more straightforward control structure with improved control performance [15]. The combination of SVPWM and carrier-based modulation techniques is incorporated for the reduction of CMV [16].

The author establishes a new technique for impedance control in the four-leg grid-connected inverter [17]. A novel

International Journal on Recent and Innovation Trends in Computing and Communication
ISSN: 2321-8169 Volume: 11 Issue: 9
***Article Received**: 25 July 2023 **Revised**: 12 September 2023 **Accepted**: 30 September 2023*

_ dual-control approach was suggested to enhance computations, offers achieving zero error with rapid regulation [18].

A quantitative analysis method was suggested for oscillation modes using the admittance network model. The method considers the dual-frequency coupling effect, sequence components coupling effect, and their interrelated relationship [19]. An enhanced SVPWM technique, consisting of three medium vectors and one zero vector, was introduced to reduce leakage currents effectively [20].

The grid-connected SPV system with an ANFIS controller is implemented to tackle the reduction of LC and CMV. Additionally, it addresses reactive power compensation for zero voltage regulation or power factor correction, along with load balancing, elimination of load harmonic currents, and mitigation of neutral current at the PCC in a four-wire distribution system. The proposed two-stage SPV generating system aims to enhance power quality. The maximum power tracking is achieved through an MPPT utilising a boost converter (BC). The SPV power is generated through a common DC link of the BC and Voltage Source Converter, and its voltage is regulated using an ANFIS. The system's effectiveness for compensating load currents is improved through the proposed configuration. The design, modelling, and performance simulation of the Solar Photovoltaic (SPV) generating system are carried out using MATLAB software.

The remaining sections of this paper are structured as follows. Section II provides an introduction to the power circuit topology and operating principles of a FNPCI and T-FNPCI PV grid-connected inverter. In Section III, a PBC is examined based on the Euler–Lagrange mathematical model. The three-level SVPWM for pulse generation is detailed in Section IV. Subsequently, Section V presents the system's performance results using a simulation platform featuring a 10-kW PV grid-connected inverter. Finally, Section VI concluding remarks for this paper.

II. PROPOSED CONFIGURATION

The structure of the solar grid-connected inverter is shown in Figure 1. The DC side of the inverter is connected to the PV via a DC-DC boost converter. TL inverters are favoured in PV grid-tied systems for their advantages, such as increased efficiency, reduced cost, and compact size. However, it's important to note that these inverters lack galvanic isolation, resulting in higher LC than isolated inverters. This increased LC leads to several issues, including elevated EMI, greater total THD, higher system losses, and safety concerns.

Inverters with four legs are used in a variety of applications, including the removal of neutral current from microgrids, the decrease of oscillations in both active and reactive power, and the maintenance of PCC line-to-line voltage in the event of microgrid breakdowns by taking control of zero sequence currents. The recently developed Passivity-based controller for 4-leg 3 Level NPCI is more efficient than linear current controllers in feeding the microgrid with imbalanced currents. The 4-leg 3 Level NPCI's redundant switching states are exploited by a passivity-based controller to balance the DC-link voltages.

A. Three-phase four-leg NPC inverter (FNPCI)

The leg-A of the proposed FNPCI is as shown in figure 2 comprises four IGBT switches (S1a to S4a) and their respective diodes.

The 'N' is established between two capacitors. Clamping diodes (D1a and D2a) are also connected to the neutral point to provide clamping functionality.

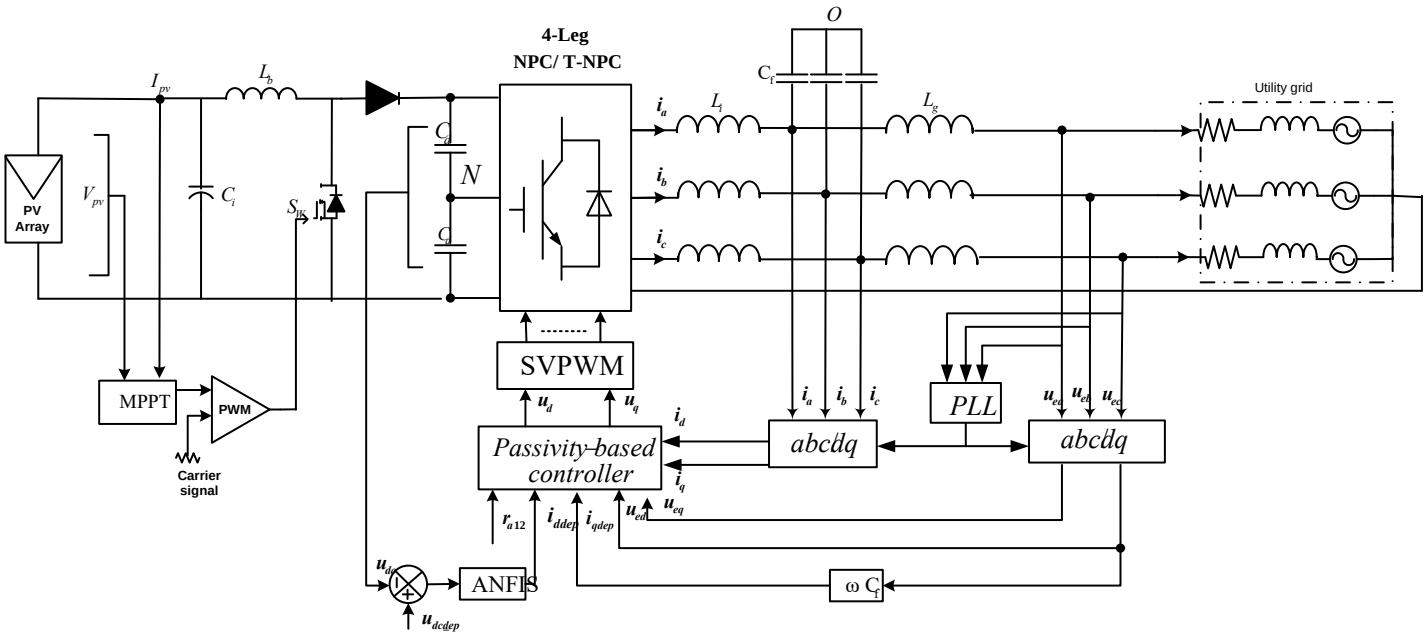

Figure 1. Block diagram of the Grid Connected Solar PV system

International Journal on Recent and Innovation Trends in Computing and Communication
ISSN: 2321-8169 Volume: 11 Issue: 9
***Article Received**: 25 July 2023 **Revised**: 12 September 2023 **Accepted**: 30 September 2023*

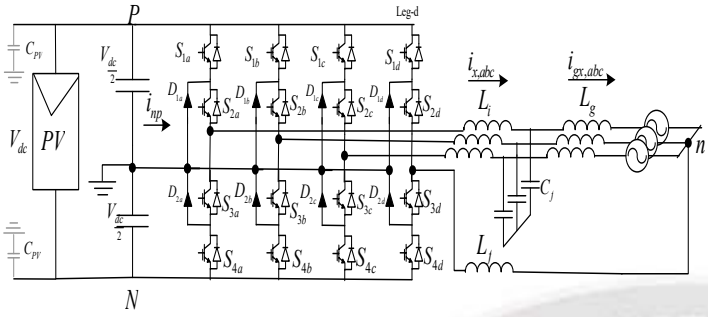

Figure 2. Three-Phase FNPCI

Table 1presents the switching states of the FNPCI along with the corresponding output voltage. An imbalance in the neutral-point voltage (NPV) might arise from the neutral current (iN) charging or discharging the capacitors, contingent upon the particular switching state and the direction of load currents.

Switching States	S_{1a}	S_{2a}	S_{3a}	S_{4a}	V_{AC}
+1	ON	ON	OFF	OFF	$V_d/2$
0	OFF	ON	ON	OFF	0
-1	OFF	OFF	ON	ON	$-V_d/2$

Table 1. Switching states of FNPCI for leg A

B. Three-phase, Four-leg TNPC Inverter (T- FNPCI)

The NPC inverter necessitates the incorporation of four IGBTs and six diodes within each phase. The breakdown voltage for the diodes is set at half of the DC link voltage (Vdc). In this arrangement, two IGBTs actively carry current in each phase simultaneously. On the contrary, the T-type NPCI, which is derived from the 3 phase 3 level NPCI, demands the inclusion of four diodes in each phase. Nevertheless, only one IGBT conducts current in each phase leg at any given time, resulting in reduced conduction losses. Consequently, the T-type NPCI exhibits greater efficiency compared to the diode-clamped NPC, especially at medium switching frequencies. The block diagram illustrating the proposed system is depicted in Figure 3.

The output voltage will be positive, when both the switches SW2a, SW3a are turned off simultaneously while SW1a is on. Similarly, deactivating SW1a, SW2a and turning on SW3a will result in the output voltage will be zero. Turning off SW1a, SW3a and activating SW2a will generate the negative output voltage. The corresponding switching states are shown in Table.2. To avoid any potential DC bus short circuit, a dead time is incorporated for all switches. This dead time ensures that there is a brief interval during which both switches are off before changing states to prevent any harmful electrical effects.

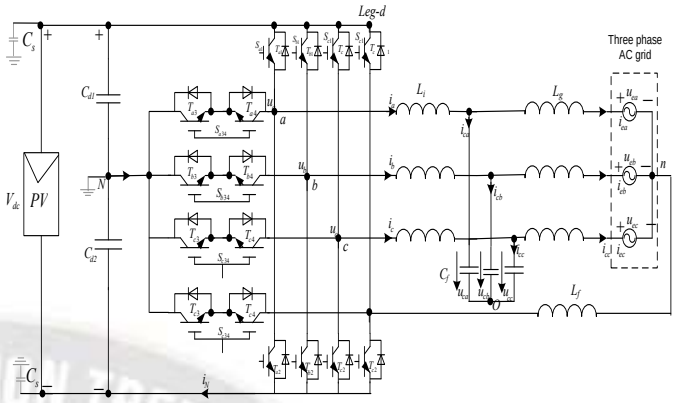

Figure 3. Three-Phase T-FNPCI

However, within the four-leg T-type NPC, the outer switches, namely SW1a and SW2a, along with their corresponding freewheeling diodes, experience relatively higher switching losses. This is attributed to the fact that they are tasked with blocking the entire DC Link voltage.

Table 2. Switching states of four leg T-FNPCI for leg A

Switching States	S_{1a}	S_{2a}	S_{3a}	V_{AC}
+1	ON	OFF	OFF	$V_d/2$
0	OFF	OFF	ON	0
-1	OFF	ON	OFF	$-V_d/2$

III. METHODOLOGY

A. Port-Controlled Hamiltonian with a Mathematical Model of a Four Leg T-NPC Inverter

From Figure 3, in accordance with KVL, the voltage equations are formulated at the grid as follows:

$$\begin{cases} L\dfrac{di_a}{dt} + Ri_a - u_{ao} = -u_{ea} \\ L\dfrac{di_b}{dt} + Ri_b - u_{bo} = -u_{eb} \\ L\dfrac{di_c}{dt} + Ri_c - u_{co} = -u_{ec} \end{cases} \quad (1)$$

where u_{ao}, u_{bo}, and u_{co} are the phase voltages of the inverter, given as

$$\begin{cases} u_{ao} = u_{aN} + u_{No} = \left(S_{a1}u_{dc1} - S_{a2}u_{dc2}\right) + u_{No} \\ u_{bo} = u_{bN} + u_{No} = \left(S_{b1}u_{dc1} - S_{b2}u_{dc2}\right) + u_{No} \\ u_{co} = u_{cN} + u_{No} = \left(S_{c1}u_{dc1} - S_{c2}u_{dc2}\right) + u_{No} \end{cases} \quad (2)$$

Combining the Eq. (1) and (2):

International Journal on Recent and Innovation Trends in Computing and Communication
ISSN: 2321-8169 Volume: 11 Issue: 9
***Article Received**: 25 July 2023 **Revised**: 12 September 2023 **Accepted**: 30 September 2023*

$$\begin{cases} L\dfrac{di_d}{dt}-\omega Li_q+Ri_d-\dfrac{(S_{d1}-S_{d2})u_{dc}}{2}-\dfrac{(S_{d1}+S_{d2})\Delta u_{dc}}{2}=-u_{ed} \\ L\dfrac{di_q}{dt}-\omega Li_d+Ri_q-\dfrac{(S_{q1}-S_{q2})u_{dc}}{2}-\dfrac{(S_{q1}+S_{q2})\Delta u_{dc}}{2}=-u_{eq} \\ \dfrac{C_d}{3}\dfrac{du_{dc}}{dt}+\dfrac{(S_{d1}-S_{d2})i_d}{2}+\dfrac{(S_{q1}-S_{q2})i_q}{2}=\dfrac{2}{3}i_D \\ \dfrac{C_d}{3}\dfrac{\Delta du_{dc}}{dt}+\dfrac{(S_{d1}+S_{d2})i_d}{2}+\dfrac{(S_{q1}+S_{q2})i_q}{2}=0 \end{cases} \quad (3)$$

Denoting ud and uq as the voltages on the dq-axis components, respectively, and they are expressed as follows:
(i)By Euler Representation: The Euler model of the T-FNPCI can be represented as follows by using Eq. (3)

$$M\dot{x}+Jx+Rx=u$$

(ii)PBC based T-FNPCI: A system is considered strictly passive if there exists a nonnegative storage function H(x) and a positive definite function Q(x), satisfying:

$$H\left(x(T)\right)-H\left(x(0)\right)\le \int_0^T u^T y d\tau-\int_0^T Q(x)d\tau,\ \ T>0 \quad (4)$$

To achieve the desired stability point, the T-FNPCI can be employed for realization, indicating that x1 → x1s, x2 → x2s, x3 → x3s, and x4 → x4s, where x1s, x2s, x3s, and x4s are the required stability factors of id, iq, Vdc, and Δ Vdc, correspondingly, i.e., xs = [x1s x2s x3s x4s] T = [ids iqs Vdcs ΔVdcs] T is the targeted vector. In line with the control specifications for the proposed configuration, ien (where n = a, b, c) is set to be in inverse phase with Ven and exhibit sinusoidal characteristics. This configuration aims to achieve a unity power factor on the grid side.
As space vectors of Vea (Veb, Vec), iea (ieb, iec), ica (icb, icc), and ia (ib, ic), correspondingly, set Ve, ie, ic, and i. Thus, the following are the necessary current vectors:

$$\begin{cases} i_{ds}=i_e \\ i_{qs}=i_c \end{cases} \quad (5)$$

where ids, iqs are calculated by PI controller, which is used to regulate the voltage effectively and it is given by

$$i_{qs}=\omega C_f V_{ed} \quad (6)$$

Based on the previously mentioned equations, the T-FNPCI desired equilibrium points are expressed as follows:

$$\begin{cases} x_{1s}=i_{ds} \\ x_{2s}=i_{qs}=\omega C_f V_{ed} \\ x_{3s}=V_{dcs}>\sqrt{3}V_{em} \\ x_{4s}=\Delta V_{dcs}=0 \end{cases} \quad (7)$$

PBC-based Controller by adding damping injection

Define the error as xerr = x – xs, and let He(x) represent the error storage operation, where

$$H_e(x)=x_e^T M x_e/2. \quad (8)$$

If He(x) converges to zero through a PBC, Xerr approaches 0, fulfilling the control objectives. According to Eq. (4), the error Euler model of the T-FNPCI can be expressed as:

$$Mx_{err}+Rx_{err}=V-(Mx_s+Jx+Rx_s) \quad (9)$$

Damping injection with Ra is essential to expedite the convergence of He(x) to zero. The dissipation due to damping injection is represented as Rdxerr = (R + Ra) xerr. The positive definite diagonal damping matrix Ra is given by Ra = diagonal {ra12, ra12, 1/ra34, 1/ra34}, where ra12 and ra34 are positive constant values. Hence, the Euler model given in Eq. (9) is modified as:

$$Mx_{err}+R_d x_{err}=V-(Mx_s+Jx+Rx_s-R_a x_{err}) \quad (10)$$

Where $V=Mx_s+Jx+Rx_s-R_a x_{err}$ (11)

Because Rd is a positive definite matrix, we have

$$\dot{H}_e(x)=x_e^T M\dot{x}_e=-x_e^T R_d x_e<0. \quad (12)$$

Eq. (12) demonstrates that He(x) approaches 0 and xerr converges to 0 through the PBC based controller. The rate at which He(x) approaches 0 is predominantly determined by Rd. When Ra ≫ R, the pace at which He(x) approaches 0 is primarily influenced by Ra. This indicates that the PBC based controller exhibits robustness against resistor parameters.

IV. STUDY OF CMV, LC BY USING SVPWM

Figure 4 presents the proposed controller's Switching pattern using SVPWM. The three-level inverter comprises a total of 27 switching states, allowing for the selection of 19 distinct voltage vectors. The voltage vectors in the inverter can be categorized into five groups, depending on their amplitudes and how they affect the capacitor voltages on the AC side.

The Adaptive Neuro-Fuzzy Inference System (ANFIS) is a hybrid computational model that merges the principles of neural networks and fuzzy logic, enabling it to make intelligent decisions and its structure is given in Figure 6. ANFIS belongs to the category of fuzzy systems and operates by employing a collection of fuzzy if-then rules to approximate nonlinear functions. To accomplish this, it employs neural network architecture for two purposes: to train the fuzzy rules and to establish a mapping between input and output data.

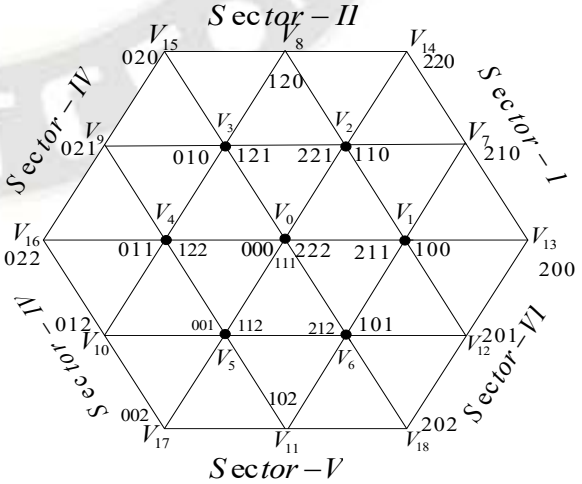

Figure 4. Voltage SV locations to different switching states

International Journal on Recent and Innovation Trends in Computing and Communication
ISSN: 2321-8169 Volume: 11 Issue: 9
Article Received: 25 July 2023 Revised: 12 September 2023 Accepted: 30 September 2023

The membership function (Msf) for Dc link voltage balancing is illustrated in table.3. The output of Msf is given in Figure 5.

TABLE.3: Msf for DC link voltage

Error	CE						
	BPS	MPS	SPS	ZR	SNG	MNG	BNG
BNG	ZR	SNG	MNG	BNE	BNG	BNG	BNG
MNG	SPS	ZR	SNG	MNG	BNG	BNG	BNG
SNG	MPS	SPS	ZR	SNG	MNG	BNG	BNG
ZR	BPS	MPS	SPS	ZR	SNG	MNG	BNG
SPS	BPS	BPS	MPS	SPS	ZR	SNG	MNG
MPS	BPS	BPS	BPS	MPS	SPS	ZR	SNG
BPS	BPS	BPS	BPS	BPS	MPS	SPS	ZR

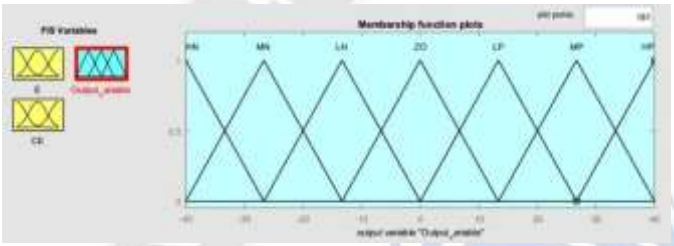

Figure 5. Msf of Output

Represented by a collection of fuzzy rules, the fuzzy logic establishes the correlation between input variables and the output variable. These fuzzy rules are subsequently employed to construct a neural network, which undergoes training via a backpropagation algorithm.

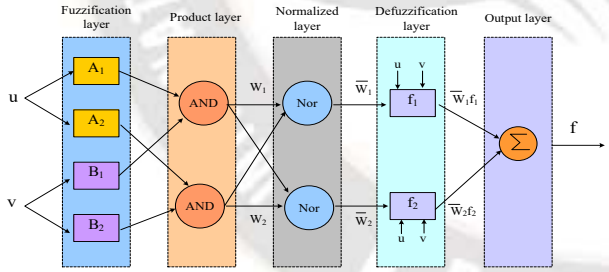

Figure 6. Structure of ANFIS

Effect of additional leg introduced in the existing system

In recent times, there has been a growing interest among researchers in the utilization of three-phase four-leg inverters due to their effectiveness in managing unbalanced loads in four-wire systems. In this topology, the neutral point is established by connecting the neutral path to the midpoint of the additional fourth leg. While this configuration eliminates the need for large and costly capacitors and results in lower ripple on the DC-link voltage, the incorporation of two additional switches introduces complexity to the control scheme.

The CMV and LC are defined as:

$$U_{CM} = (U_{AN} + U_{BN} + U_{CN} + U_{DN})/4 \quad (13)$$

$$i_{CM}(t) = -C_{PV}\frac{du_{PV}(t)}{dt} \quad (14)$$

As indicated in Eq. (14), it is evident that the LC is influenced by both the parasitic capacitance of Cpv and the duPV(t)/dt. In practical scenarios, the parasitic capacitance is uncertain and varies due to factors like humidity, weather conditions, dust accumulation on the PV panel, and other environmental elements. Nonetheless, the parasitic capacitance typically assumes a relatively small value, for instance, 220 nF.

V. SIMULATION RESULTS

The proposed FNPCI and T-FNPCI were developed in MATLAB Simulink environment. The grid voltage and current waveforms, the LC and CMV, the active and reactive powers were analysed for each proposed configuration. In addition, the THD was obtained and further, it is compared with ANFIS controller.

In Figure 7(a), the sinusoidal form of the grid voltage and current is depicted, with magnitudes of 380V and 22A, respectively. The waveform for grid voltage and current of FNPC is shown in Figure 7(a) and its LC and CMV waveforms are shown in Figure 7(b) & (c) respectively. Moving on to Figure 8(a), it showcases the grid voltage and current waveforms, with magnitudes of approximately 380V and 20A for T-FNPCI. Meanwhile, Figure 8(b) and 8(c) displays its LC and CMV waveforms respectively. It can be observed that from Figure 7, and Figure 8, the incorporation of the fourth leg effectively reduces the magnitudes of LC and CMV. The line-to-line voltage waveform for leg A of the proposed inverter configuration is as shown in Figure 9. However, Figure 10 depicts the UPF waveform, sector generation with SVPWM technique and its pulses are given in Figure 11 and Figure 12 respectively.

Furthermore, Figure 13 shows the DC Link voltage waveform under various solar irradiation values and at a constant temperature, using ANFIS controller. It is evident that the ANFIS controller achieves a faster settling time, resulting in a constant voltage across the DC Link voltage. Figure 14 shows the active power and reactive powers of proposed system. The THD spectrum for grid current with ANFIS controller is as shown in Figure 15. It can be evident that the THD with ANFIS controller is less compared to the PI controller for the proposed system. Table 4 is a summary of the system's parameters to verify the proposed system by using PBC-based control method.

TABLE.4: Ratings of proposed system

.No.	Parameter	Value
1	PV Power	10 kW
2	Boost converter L, C	5 mH, 1200 µF
3	Input DC voltage (Vdc)	700 V
4	Capacitors (C1 and C2)	470 µF
5	Filter inductance (Linv, Lgrid)	2.5 mH, 2.3mH
6	Filter Capacitance (Cf)	4 µF
7	Load resistance (R)	10 Ω
8	Nominal Frequency	50 Hz
9	Sampling Time (Ts)	50 µs

International Journal on Recent and Innovation Trends in Computing and Communication
ISSN: 2321-8169 Volume: 11 Issue: 9
***Article Received**: 25 July 2023 **Revised**: 12 September 2023 **Accepted**: 30 September 2023*

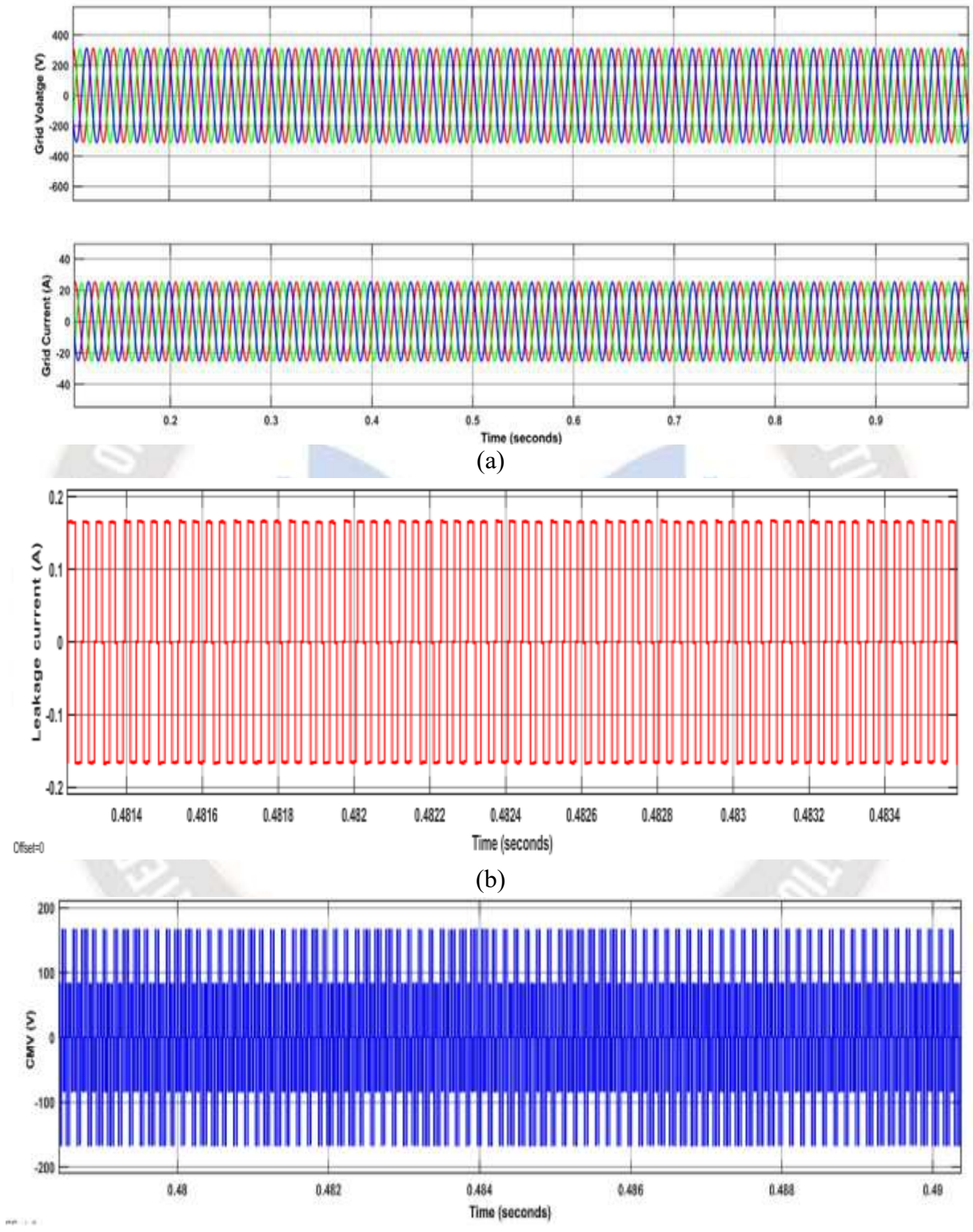

Figure 7. (a) Output Grid Voltage and Grid Current waveforms (b) Waveform for LC (c) CMV generated by SVPWM technique for FNPCI

International Journal on Recent and Innovation Trends in Computing and Communication
ISSN: 2321-8169 Volume: 11 Issue: 9
Article Received: 25 July 2023 Revised: 12 September 2023 Accepted: 30 September 2023

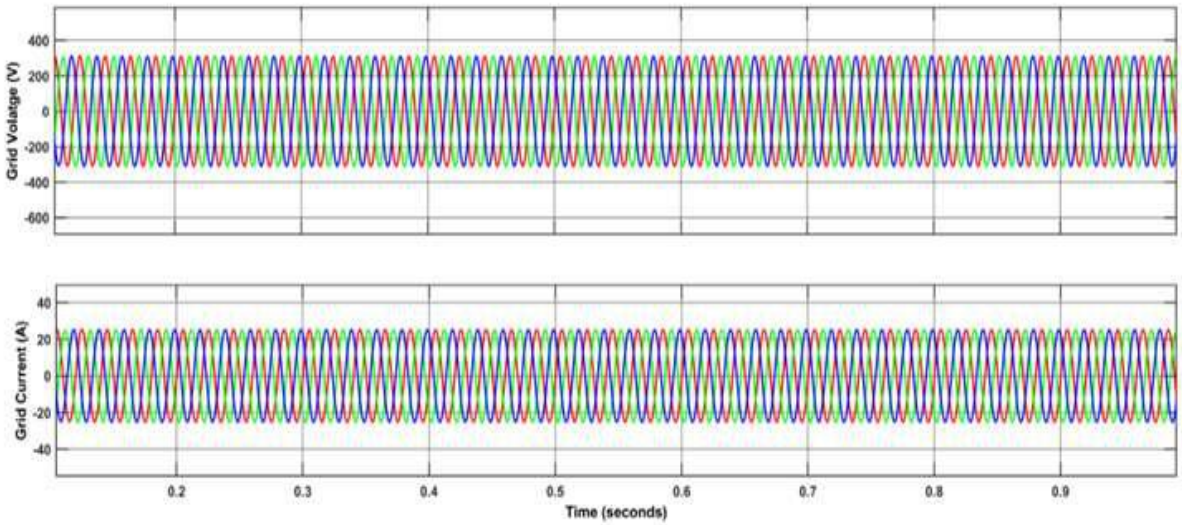

(a)

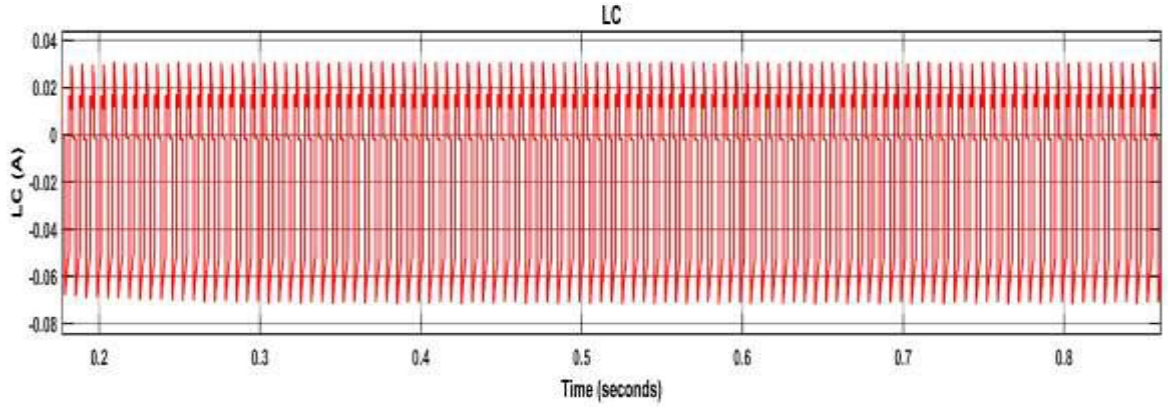

(b)

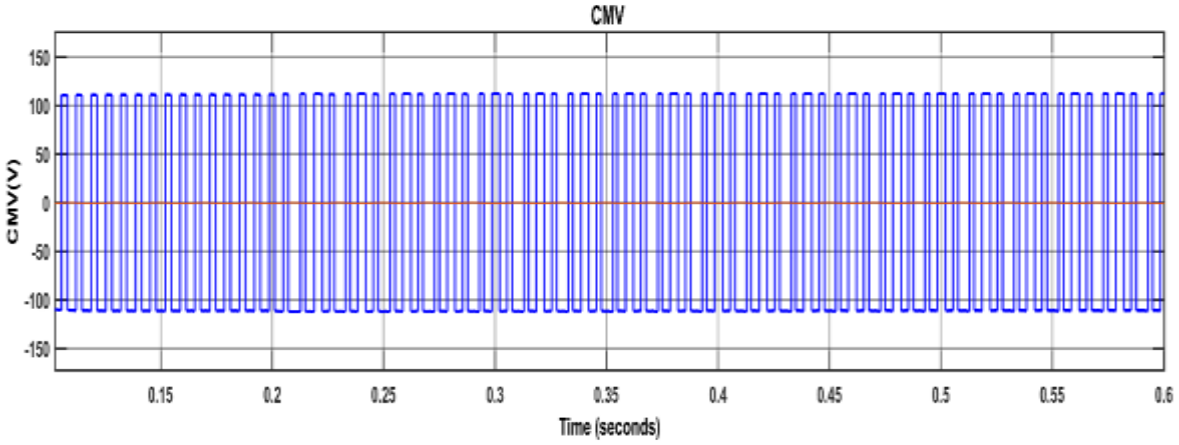

(c)

Figure 8 (a) Output Grid Voltage and Grid Current waveforms (b) Waveform for LC (c) CMV generated by SVPWM technique for T-FNPCI

International Journal on Recent and Innovation Trends in Computing and Communication
ISSN: 2321-8169 Volume: 11 Issue: 9
Article Received: 25 July 2023 Revised: 12 September 2023 Accepted: 30 September 2023

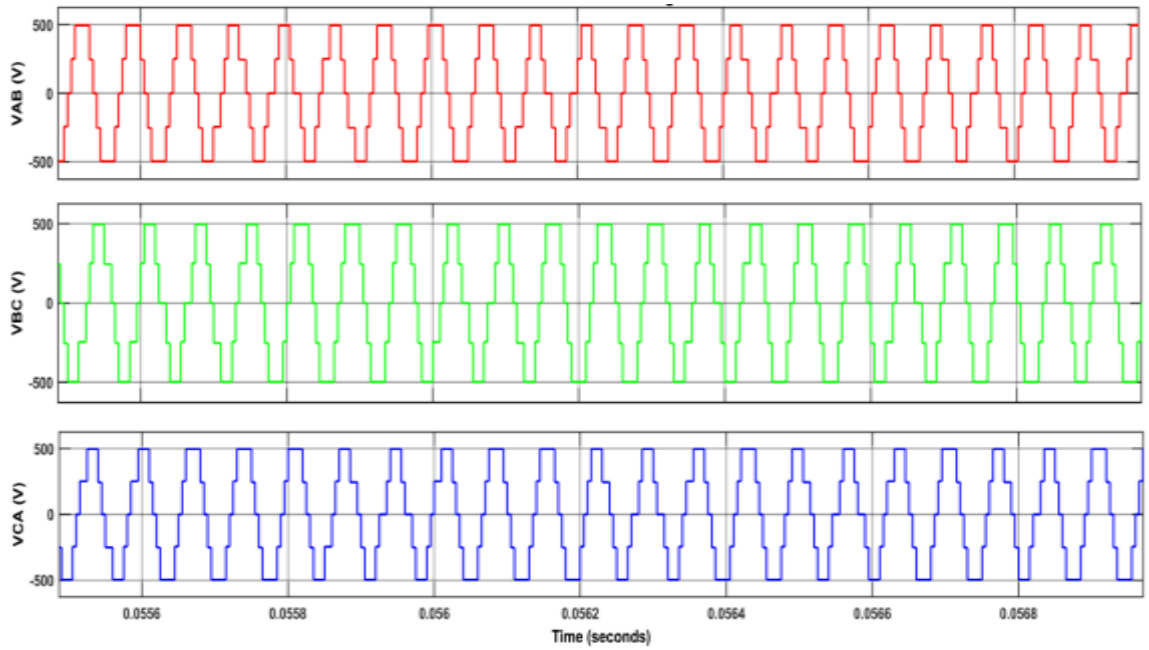

Figure 9. Output line-line voltages

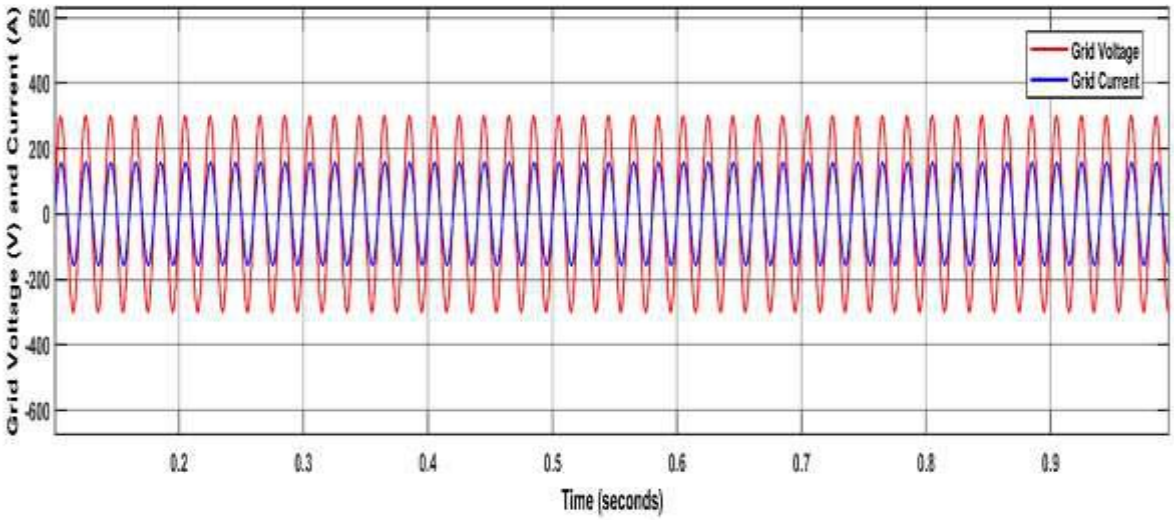

Figure 10. Waveform of UPF

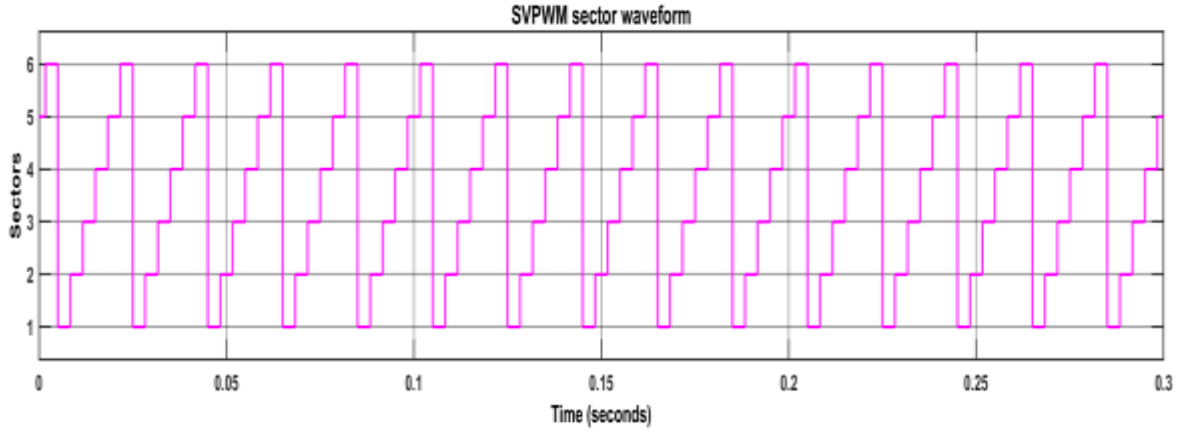

Figure 11. Sector Generation by SVPWM

International Journal on Recent and Innovation Trends in Computing and Communication
ISSN: 2321-8169 Volume: 11 Issue: 9
Article Received: 25 July 2023 Revised: 12 September 2023 Accepted: 30 September 2023

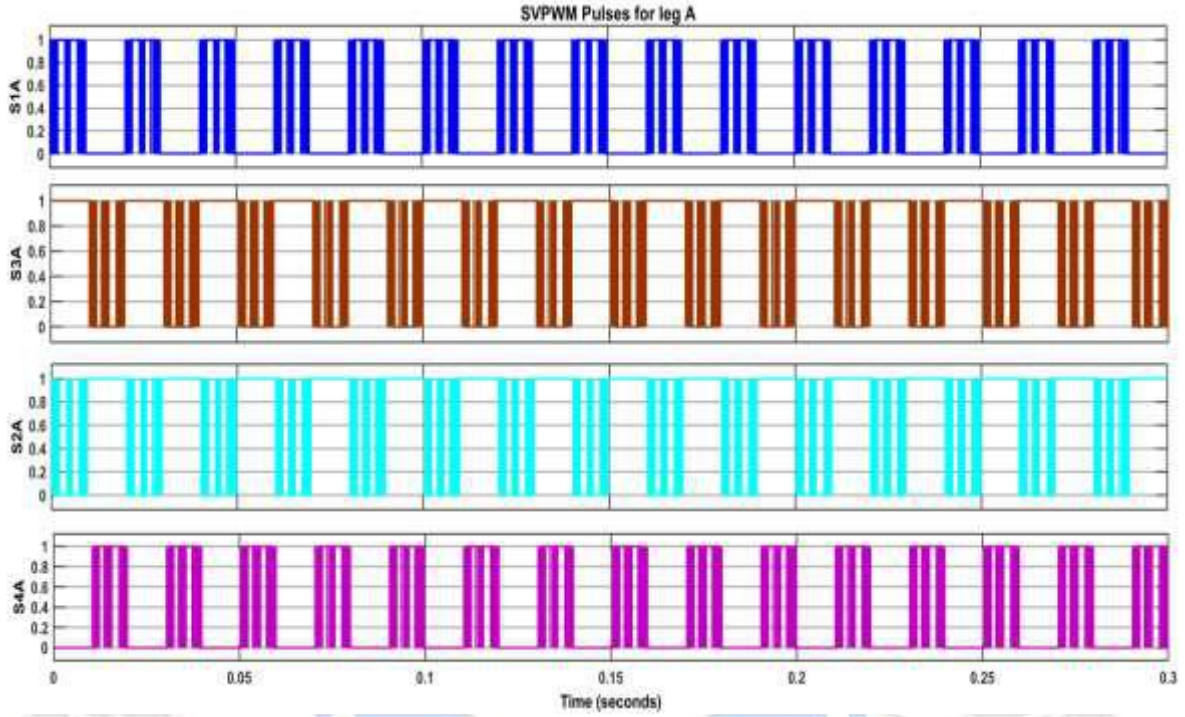

Figure 12. SVPWM pulses

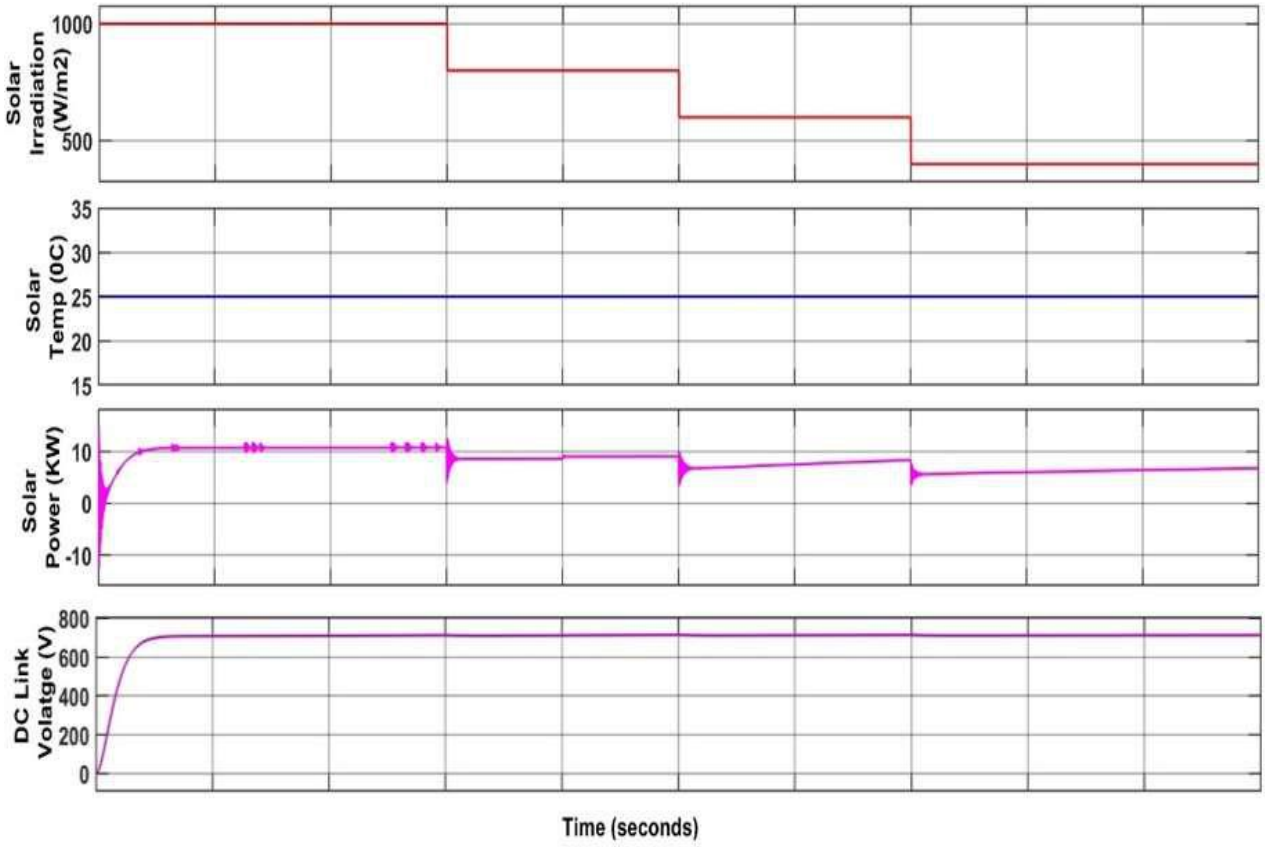

Figure 13. DC inkL voltage waveform at different solar irradiances of proposed configuration using ANFIS controller

International Journal on Recent and Innovation Trends in Computing and Communication
ISSN: 2321-8169 Volume: 11 Issue: 9
Article Received: 25 July 2023 Revised: 12 September 2023 Accepted: 30 September 2023

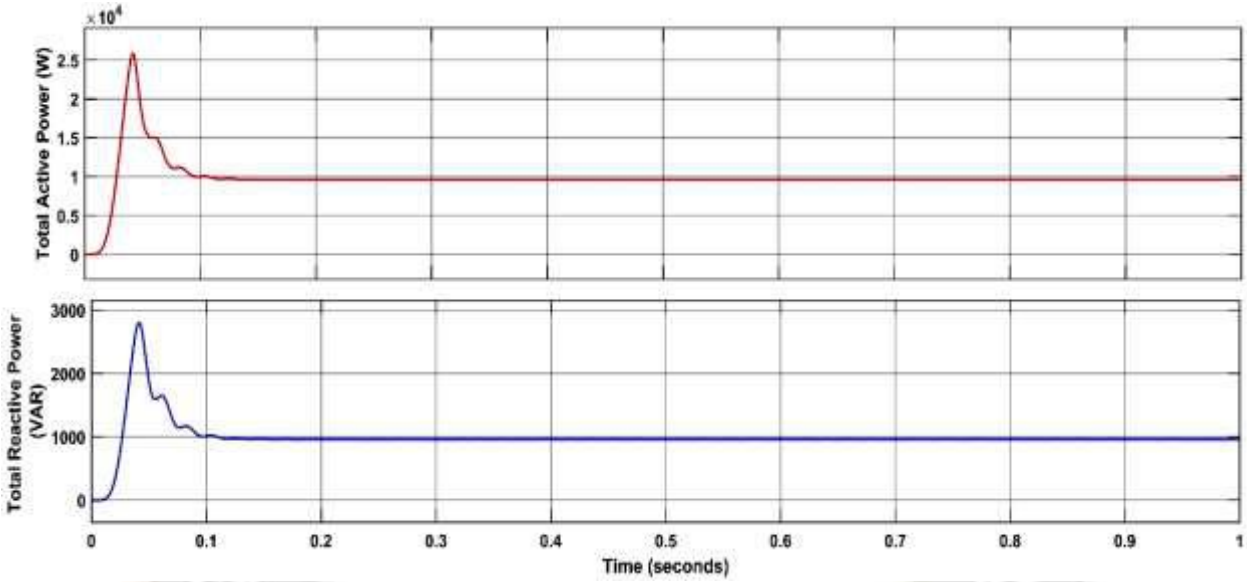

Figure 14. Active power and Reactive powers

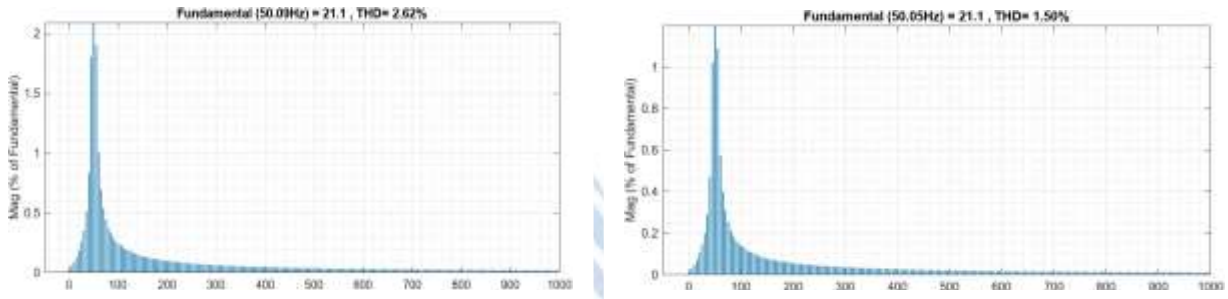

(a) (b)

Figure 15. Grid current THD using ANFIS control (a) FNPCI (b) T-FNPCI

Table 5. Comparison table for proposed systems

S.No	Parameters		FNPCI	T-FNPCI
1	PV array output voltage before boost converter		362.9 V	362.9 V
2	PV array output voltage after boost converter		725 V	700 V
3	Common mode voltage		180 V	105 V
4	Leakage current		150 mA	30 mA
5	Inverter output voltage(Line)		579V	500 V
6	Grid voltage(phase), rms		292 V	300 V
7	Grid current		23 A	20 A
8	Grid THD	Voltage THD	0.38%	0.13%
		Current THD	1.00%	0.14%

V. CONCLUSION

This article introduces a novel configuration incorporating both a FNPCI and a T-FNPCI, utilizing a passivity-based control technique. The T-FNPCI is particularly effective in reducing both Common Mode Voltage (CMMV) and Leakage Current (LC) while minimizing the required number of switches when compared to the FNPCI. These characteristics make it highly suitable for grid-connected applications, ensuring safe and reliable operation.

Additionally, we have integrated an ANFIS controller with the SVPWM technique in the proposed configuration to maintain a constant voltage across the DC Link amidst varying solar irradiation and temperature conditions. This integration results in high-quality inverter-side output currents with low Total Harmonic Distortion (THD). Notably, the ANFIS controller exhibits its superiority in DC Link voltage regulation by achieving a faster settling time when compared to the conventional Proportional-Integral (PI) controller.

REFERENCES

[1] Sen, Z.: 'Solar energy fundamentals and modeling techniques atmosphere, environment, climate change and renewable energy' (Springer-Verlag London Limited, 2008).

[2] Teodorescu, R., Liserre, M., Rodriguez, P.: 'Grid converters for photovoltaic and wind power system' (John Wiley & Sons, Ltd, The Atrium, Southern Gate, Chichester, West Sussex, UK, 2011).

[3] S. R. Mohapatra and V. Agarwal, "Enhancement of Line-to-Line Voltage Support During Asymmetrical Microgrid Faults Using a Four-Leg Three-Level Inverter," in IEEE Transactions on Smart Grid, vol. 13, no. 2, pp. 1298-1309, March 2022, doi: 10.1109/TSG.2021.3130745.

[4] Koutroulis, E., Blaabjerg, F.: 'Methodology for the optimal design of transformer less grid-connected PV inverters', IET Power Electron., 2012, 5, (8), pp. 1491–1499.

[5] Li, J., Zhuo, F., Wang, X., Wang, L., Ni, S.: 'A grid-connected PV system with power quality improvement based on boost + dual-level four-leg inverter'. Proc. IEEE Sixth Int. Power Electronics and Motion Control Conf. 2009 (IPEMC '09), 17–20 May 2009, pp. 436–440.

[6] Balathandayuthapani, S., Edrington, C.S., Henry, S.D., Cao, J.: 'Analysis and control of a photovoltaic system: application to a high-penetration case study', IEEE Syst. J., 2012, pp. 213–219.

[7] Jain, S., Agarwal, V.: 'Comparison of the performance of maximum power point tracking schemes applied to single-stage grid-connected photovoltaic systems', IET Electric Power Appl., 2007, 1, (5), pp. 753–762.

[8] Subudhi, B., Pradhan, R.: 'A comparative study on maximum power point tracking techniques for photovoltaic power systems', IEEE Sust. Energy, 2013, 4, (1), pp. 89–98.

[9] Dejia, Z., Zhengming, Z., Eltawil, M., Liqiang, Y.: 'Design and control of a three-phase grid-connected photovoltaic system with developed maximum power point tracking'. IEEE Applications on Power Electronics Conf. and Exposition, APEC 2008, May 2008, pp. 973–979.

[10] dos Santos, E.C., Jacobina, C.B., Rocha, N., Dias, J.A.A., Correa, M.B. R.: 'Single-phase to three-phase four-leg converter applied to distributed generation system', IET Power Electron., 2010, 3, (6), pp. 892–903.

[11] Shen, J.-M., Jou, H.-L., Wu, J.-C.: 'Transformer-less three-port grid-connected power converter for distribution power generation system with dual renewable energy sources', IET Power Electron., 2012, 5, (4), pp. 501–509.

[12] Singh, B., Solanki, J.: 'A comparison of control algorithms for DSTATCOM', IEEE Trans. Ind. Electron., 2009, pp. 2738–2745.

[13] Mikkili, S., Panda, A.K.: 'Simulation and real-time implementation of shunt active filter id-iq control strategy for mitigation of harmonics with different fuzzy membership functions', IET Power Electron., 2012, 5, (9), pp. 1856–1872.

[14] B. Sharma et al., "Power Sharing in Three-Level NPC Inverter Based Three-Phase Four-Wire Islanding Microgrids with Unbalanced Loads," in IEEE Access, vol. 11, pp. 20725-20740, 2023, doi: 10.1109/ACCESS.2023.3250219.

[15] G. Tan, J. Wei, W. Zhao, L. Qi and X. Sun, "Application of Three-Dimensional Unbalanced Coordinate Transformation to Stand-Alone Four-Leg Voltage-Source Inverter," in IEEE Transactions on Power Electronics, vol. 37, no. 10, pp. 11686-11703, Oct. 2022, doi: 10.1109/TPEL.2022.3173396.

[16] L. Zhang, H. Yang, P. Tu and Y. Tang, "Decoupled Modulation Scheme for Three-Phase Four-Leg Four-Wire Three-Level T-Type Inverter," 2021 IEEE Energy Conversion Congress and Exposition (ECCE), Vancouver, BC, Canada, 2021, pp. 3407-3411, doi: 10.1109/ECCE47101.2021.9595573.

[17] H. Nian, Y. Liao, M. Li, D. Sun, Y. Xu and B. Hu, "Impedance Modeling and Stability Analysis of Three-Phase Four-Leg Grid-Connected Inverter Considering Zero-Sequence," in IEEE Access, vol. 9, pp. 83676-83687, 2021, doi: 10.1109/ACCESS.2021.3087331.

[18] M. Yang, W. Cao, J. Zhao, J. Song and L. Wei, "Dual Current Control Loops for Three-Phase Four-Leg Grid-Connected Inverter using Complex-Vector Form," 2021 IEEE 1st International Power Electronics and Application Symposium (PEAS), Shanghai, China, 2021, pp. 1-4, doi: 10.1109/PEAS53589.2021.9628767.

[19] Y. Liao, Y. Wang, H. Nian, H. Li, Y. Qiu and D. Sun, "A Stability Quantitative Analysis Method of Three-Phase Four-Wire Grid-Connected Systems Considering Frequency Coupling and Sequence Components Coupling," in IEEE Access, vol. 11, pp. 99237-99252, 2023, doi: 10.1109/ACCESS.2023.3313777.

[20] M. C. Cavalcanti, A. M. Farias, K. C. Oliveira, F. A. S. Neves and J. L. Afonso, "Eliminating Leakage Currents in Neutral Point Clamped Inverters for Photovoltaic Systems," in IEEE Transactions on Industrial Electronics, vol. 59, no. 1, pp. 435-443, Jan. 2012, doi: 10.1109/TIE.2011.2138671